European Journal of Mechanics A/Solids 30 (2011) 432–441

Contents lists available at ScienceDirect

European Journal of Mechanics A/Solids

journal homepage: www.elsevier.com/locate/ejmsol

Free vibration and dynamic stability of rotating thin-walled composite beams

C. Martín Saravia [a,b,*], Sebastián P. Machado [a,b], Víctor H. Cortínez [a,b]

[a] Grupo Análisis de Sistemas Mecánicos, Centro de Investigaciónes en Mecánica Teórica y Aplicada, Universidad Tecnológica Nacional, Facultad Regional Bahía Blanca, 11 de Abril 461, Bahía Blanca B8000LMI, Argentina
[b] CONICET, Av. Rivadavia 1917, Buenos Aires C1033AAJ, Argentina

ARTICLE INFO

Article history:
Received 14 October 2009
Accepted 22 December 2010
Available online 30 December 2010

Keywords:
Thin-walled rotating beams
Composite
Finite elements
Parametric resonance

ABSTRACT

The dynamic stability behavior of thin-walled rotating composite beams is studied by means of the finite element method. The analysis is based on Bolotin's work on parametric instability for an axial periodic load. The influence of fiber orientation and rotating speeds on the natural frequencies and the unstable regions is studied for symmetrically balanced laminates. The regions of instability are obtained and expressed in non-dimensional terms. The "modal interchange" phenomenon arising in rotating beams is described. The dynamic stability problem is formulated by means of linearizing a geometrically nonlinear total Lagrangian finite element with seven degrees of freedom per node. This finite element formulation is based on a thin-walled beam theory that takes into account several non-classical effects such as anisotropy, shear flexibility and warping inhibition.

1. Introduction

In the study of the dynamic behavior of structures, the characterization of the stability of motion plays a crucial role. With the recent technological advances in composite materials, the use of composite structures in the design of mechanical systems has been increasing fast during the last years. Due to their outstanding engineering properties, such as high strength/stiffness to weight ratios and favorable fatigue characteristics, thin-walled beams made of composite materials are widely used in the design of aircraft wings, helicopter rotor blades, wind turbine blades and the like. The structural configuration possibilities provided by fiber reinforced composite materials are vital to enhance the dynamic behavior of rotating beams operating in complex environmental conditions. As a result of the mentioned advances in composite materials, the structural design concepts have changed substantially. Thus, a complete understanding of the behavior of structures that work under dynamical load conditions is essential.

The problem of dynamic instability of elastic structural elements, such as rods, beams and columns, induced by parametric excitation has been addressed by many researchers. Early work on this subject was reported by Evan-Iwanowski (1965) and Nayfeh and Mook (1979). Bolotin (1964) provided an extensive introduction to the analysis of dynamic stability problems of various structural elements.

Solving the parametric vibration problem of a beam subjected to a compressive dynamic force leads to the well-known Mathieu-Hill equation (Bolotin, 1964; Evan-Iwanowski, 1965). Nayfeh and Mook (1979) used a perturbation method to solve this equation, in order to analyze the behavior of an elastic system under parametric excitation, establishing a criterion to obtain the transition curves by determining the characteristic exponents in the solution.

In relation to thin-walled beams, Goldenblat (1947) investigated the problem of the stability of a compressed thin-walled rod presenting symmetry about one axis. The problem was reduced to a system of two differential equations. Tso (1968) studied the problem of longitudinal-torsional stability, while Mettler (1962) and Ghobarah and Tso (1972) analyzed the problem of bending-torsional stability of thin-walled beams. Bolotin (1953, 1964) and Popelar (1972) discussed the dynamic stability of thin-walled beams; typical I and H sections were considered. Hasan and Barr (1974) evaluated regions of instability of thin-walled beams of equal angle-section, considering axial and transverse excitation in a cantilever beam. Also, Gürgöze (1985) studied the effect of pretwist in the dynamic stability behavior of beams subjected to axial pulsating loads.

The effect of rotation on the dynamic stability behavior of beams was first analyzed by Abbas (1986). He toke into account the effect of rotary inertia and shear deformation on the stability dynamic response of the beam. Also, Chen and Peng (1995) studied the stability behavior of a rotating blade subjected to axial load. Sakar and Sabuncu (2003) studied the coupling effects in the dynamic stability of rotating asymmetric cross-section blades. In relation to composite materials, Chen and Peng (1998) investigated the

* Corresponding author. CONICET, Av. Rivadavia 1917, Buenos Aires C1033AAJ, Argentina.
E-mail address: msaravia@conicet.gov.ar (C.M. Saravia).
URL: http://www.frbb.utn.edu.ar/gasm

0997-7538/$ – see front matter © 2010 Elsevier Masson SAS. All rights reserved.
doi:10.1016/j.euromechsol.2010.12.015

dynamic stability of rotating composite shafts under axial periodic loads.

Although a number of authors have investigated the problem of dynamic stability of beams, a few works were focused on rotating thin-walled beams. In spite of the practical interest and future potential of the thin-walled composite beam structures, particularly in the context of aerospace and mechanical applications, the main body of the available investigations has been devoted to study the dynamic stability of isotropic beams. To our knowledge, no work has been done about composite rotating thin-walled beams. This problem is addressed in this paper.

The influence of rotation in the dynamic stability behavior of composite thin-walled beams subjected to axial periodic excitation is investigated. In order to determine the instability regions, the Bolotin's method is employed. The effect of the rotational speed and the static load parameter on the unstable regions is analyzed for different laminate stacking sequences. The modal interchange phenomenon arising when considering rotation stiffening effects is studied as well.

A geometrically nonlinear total Lagrangian finite element with linear interpolation and seven degrees of freedom is formulated. The numerical formulation of the dynamic stability problem is obtained by linearizing the proposed nonlinear finite element. The element matrices are obtained from a thin-walled beam theory that assumes a linear displacement field and a nonlinear strain field (Cortínez and Piovan, 2002) and considers shear and warping deformations and rotary inertia effects. This formulation is easily extendable to a full nonlinear thin-walled beams theory developed from the proposition of full nonlinear displacement field (Machado and Cortínez, 2005, 2007).

2. Kinematics

2.1. Displacement field

The present structural model is based on the following assumptions:

(1) The cross-section contour is rigid in its own plane.
(2) The warping distribution is assumed to be given by the Saint-Venant function for isotropic beams.
(3) Shell force and moment resultants corresponding to the circumferential stress σ_{ss} and the force resultant corresponding to γ_{xs} are neglected.
(4) The curvature at any point of the shell is neglected.
(5) Twisting linear curvature of the shell is expressed according to the classical plate theory.
(6) The laminate stacking sequence is assumed to be symmetric and balanced, or especially orthotropic (Barbero, 1999).

Consider two states of the beam, an undeformed reference state and a deformed state as shown in Fig. 1.

The displacement of any point in the deformed beam measured with respect to the undeformed reference state can be expressed in a global coordinate system (x, y, z) in terms of three components. A second coordinate system (X, Y, Z), where X is a running length coordinate along the reference line of the beam, is fixed to the beam cross-section. For convenience, we choose the reference line to be the locus of cross-sectional inertia centroids. The origin of (X, Y, Z) (O) is located on the reference line of the beam and is called: *pole* (Librescu, 2006). The cross-section of the beam is arbitrary and initially located perpendicular to reference line of the beam.

The kinematic behavior of the 3D beam is represented by the superposition of two movements; a translation $\boldsymbol{u}$ of the pole O (also the origin of (X, Y, Z)) measured with respect to the reference state and a rigid rotation of the cross-section about the pole (see Fig. 2).

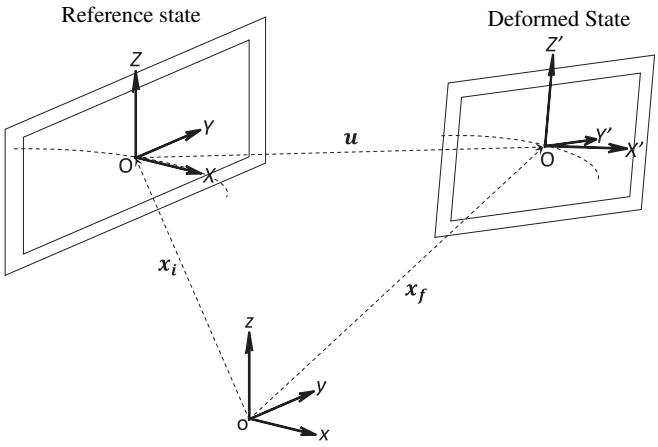

Fig. 1. Beam deformation schematic.

Thus, the resulting displacements of a point P in the cross-section will be the sum of the displacement $\boldsymbol{u} = (u, v, w)$ generated by the translation of the pole plus the additional displacements generated by the rotation of the cross-section about the pole (see Fig. 2). Thus, when the cross-section rotates about the pole the coordinate system (X, Y, Z) transforms to (X', Y', Z'). Also, an extra displacement in the longitudinal direction caused by warping is considered.

The geometry of the cross-section of the beam is defined in a curvilinear coordinate system (n,s) as:

$$Y(s,n) = Y_m(s) - n\frac{dZ_m}{ds}, Y(s,n) = Z_m(s) + n\frac{dY_m}{ds}, \tag{1}$$

where the subscript m denotes a mid-surface variable.

Introducing variables for the rotations of the cross-section about the pole and the warping displacements along the reference axis of the beam, the displacement in the curvilinear system takes the form:

$$\begin{aligned} u_x(x,s,n) &= u - \theta_z y - \theta_y z = u - \theta_z\left(Y - n\tfrac{dZ}{ds}\right) - \theta_y\left(Z - n\tfrac{dY}{ds}\right) + F\psi \\ u_y(x,s,n) &= v - \theta_x z = v - \theta_x\left(Z - n\tfrac{dY}{ds}\right) \\ u_z(x,s,n) &= w + \theta_x y = w - \theta_x\left(Y - n\tfrac{dZ}{ds}\right) \end{aligned} \tag{2}$$

where $\theta_x, \theta_y, \theta_z$ and θ represent rotations about the X, Y and Z axes and warping.

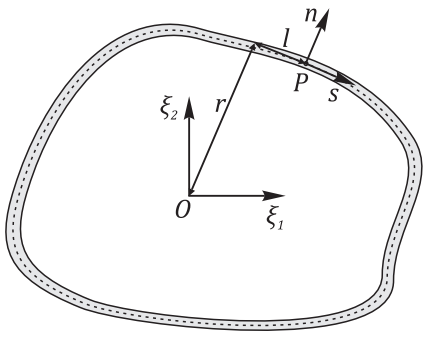

Fig. 2. Curvilinear transformation schematic.

The warping function F of the thin-walled cross-section may be defined as:

$$F(s,n) = F_P(s) + F_S(s,n) \tag{3}$$

where $F_P(s)$ and $F_S(s)$ are the contour warping function and the thickness warping function, respectively. They are defined in the form (Cortínez and Piovan, 2002; Piovan and Cortínez, 2005):

$$\begin{aligned} F_P &= \frac{1}{S}\int_0^S \left(\int_{s_0}^{s} (r(\sigma) - \Psi(\sigma))d\sigma \right) ds - \int_{s_0}^{s} (r(\sigma) - \Psi(\sigma))d\sigma \\ F_S(s,n) &= -n\, l(s), \end{aligned} \tag{4}$$

where σ is a dummy variable, and:

$$\begin{aligned} r(s) &= -Z(s)\frac{dY}{ds} + Y(s)\frac{dZ}{ds} \\ l(s) &= Y(s)\frac{dY}{ds} + Z(s)\frac{dZ}{ds} \end{aligned} \tag{5}$$

$r(s)$ represents the perpendicular distance from the shear center (SC) to the tangent at any point of the mid-surface contour, and $l(s)$ represents the perpendicular distance from the shear center (SC) to the normal at any point of the mid-surface contour, as shown in Fig. 2.

In the Eq. (4) Ψ is the shear strain at the middle line, obtained by means of the Saint-Venant theory of pure torsion for isotropic beams, and normalized with respect to $d\phi/dx$. For the case of open sections $\Psi = 0$.

3. Stress and strain fields

3.1. Strain field

The displacements with respect to the curvilinear system (x, s, n) are obtained by means of the following expressions:

$$\begin{aligned} U &= u_x(x,s,n) \\ V &= u_y(x,s,n)\frac{dY}{ds} + u_z(x,s,n)\frac{dZ}{ds} \\ W &= -u_y(x,s,n)\frac{dZ}{ds} + u_z(x,s,n)\frac{dY}{ds} \end{aligned} \tag{6}$$

The three non-zero components ε_{xx}, ε_{xs}, ε_{xn} of the Green's strain tensor are given by:

$$\begin{aligned} \varepsilon_{xx} &= \frac{\partial U}{\partial x} + \frac{1}{2}\left[\left(\frac{\partial U}{\partial x}\right)^2 + \left(\frac{\partial V}{\partial x}\right)^2 + \left(\frac{\partial W}{\partial x}\right)^2 \right] \\ \varepsilon_{xs} &= \frac{1}{2}\left[\frac{\partial U}{\partial s} + \frac{\partial V}{\partial x} + \frac{\partial U}{\partial x}\frac{\partial U}{\partial s} + \frac{\partial V}{\partial x}\frac{\partial V}{\partial s} + \frac{\partial W}{\partial x}\frac{\partial W}{\partial s} \right] \\ \varepsilon_{xn} &= \frac{1}{2}\left[\frac{\partial U}{\partial n} + \frac{\partial W}{\partial x} + \frac{\partial U}{\partial x}\frac{\partial U}{\partial n} + \frac{\partial V}{\partial x}\frac{\partial V}{\partial n} + \frac{\partial W}{\partial x}\frac{\partial W}{\partial n} \right] \end{aligned} \tag{7}$$

Substituting Eq. (2) first into Eq. (6), the resulting expression into Eq. (7) and employing the relations expressed in Eq. (1) and Eqs. (3–5) (after simplifying some higher order terms) the components of the strain tensor are expressed in the following form:

$$\begin{aligned} \varepsilon_{xx} &= \varepsilon_{xx} + n\kappa_{xx} \\ \varepsilon_{xs} &= 2\varepsilon_{xs} = \gamma_{xs} + n\kappa_{xs} \\ \varepsilon_{xn} &= 2\varepsilon_{xn} = \gamma_{xn} \end{aligned} \tag{8}$$

Where

$$\begin{aligned} \varepsilon_{xx} &= u' - Y\theta_z' - Z\theta_y' + F_P\psi' + \frac{1}{2}\left(v'^2 + w'^2\right) + \frac{1}{2}\theta_x'^2\left(Y^2 + Z^2\right) \\ \kappa_{xx} &= \frac{dZ}{ds}\theta_z' - \frac{dY}{ds}\theta_y' - l\psi' - r\theta_x'^2 \\ \gamma_{xs} &= \frac{dY}{ds}(v' - \theta_z) + \frac{dZ}{ds}(w' - \theta_y) + (r - \Psi)(\psi' - \theta_x) + \Psi\psi' \\ \kappa_{xs} &= -2\psi' \\ \gamma_{xn} &= \frac{dZ}{ds}(v' - \theta_z) + \frac{dY}{ds}(w' - \theta_y) + l(\psi' - \theta_x) \end{aligned} \tag{9}$$

The prime symbol denotes derivation with respect to the longitudinal coordinate. Keeping from the above equations only the nonlinear terms corresponding to the axial-bending and axial-torsion couplings we can express the Green-Lagrange Strain in vector form is:

$$\boldsymbol{\epsilon_R}(x,s) = [\varepsilon_{xx}, \gamma_{xs}, \gamma_{xn}, \varkappa_{xn}, \varkappa_{xn}]^T \tag{10}$$

In the derivation of the finite element matrices we split in two parts the deformation field obtained below by separating the geometric parameters related to the cross-section from Eqs. (9). Thus we can express the strain field in matrix form as:

$$\begin{bmatrix} \varepsilon_{xx} \\ \gamma_{xs} \\ \gamma_{xn} \\ \varkappa_{xn} \\ \varkappa_{xn} \end{bmatrix} = \begin{bmatrix} 1 & 0 & 0 & -Z & -Y & 0 & 0 & F_p & Y^2+Z^2 \\ 0 & Y' & Z' & 0 & 0 & \Psi & r-\Psi & 0 & 0 \\ 0 & -Z' & Y' & 0 & 0 & 0 & l & 0 & 0 \\ 0 & 0 & 0 & -Y' & Z' & 0 & 0 & -l & -2r \\ 0 & 0 & 0 & 0 & 0 & -2 & 0 & 0 & 0 \end{bmatrix} \times \begin{bmatrix} u' + \frac{1}{2}(v'^2 + w'^2) \\ v' - \theta_z \\ w' - \theta_y \\ \theta_y' \\ \theta_z' \\ \theta_x' \\ \theta_x' - \psi \\ \psi' \\ \frac{1}{2}\theta_x'^2 \end{bmatrix} \tag{11}$$

This is:

$$\boldsymbol{\epsilon_R}(x,s) = \boldsymbol{S}(s)\boldsymbol{\epsilon_G}(x) \tag{12}$$

where $\boldsymbol{\varepsilon_G}$ is the generalized strain vector, a function of the longitudinal coordinate of the beam, and $\boldsymbol{S}$ is the cross-sectional matrix

3.2. Stresses

The shell stress resultants are defined in terms of constitutive equations of symmetrically balanced laminates (Barbero, 1999) as:

$$\begin{bmatrix} N_{xx} \\ N_{xs} \\ N_{xn} \\ M_{xx} \\ M_{xs} \end{bmatrix} = \begin{bmatrix} C_{11} & 0 & 0 & 0 & 0 \\ 0 & C_{22} & 0 & 0 & 0 \\ 0 & 0 & C_{33} & 0 & 0 \\ 0 & 0 & 0 & C_{44} & 0 \\ 0 & 0 & 0 & 0 & C_{55} \end{bmatrix} \begin{bmatrix} \varepsilon_{xx} \\ \gamma_{xs} \\ \gamma_{xn} \\ \varkappa_{xx} \\ \varkappa_{xs} \end{bmatrix} \tag{13}$$

We can express the above relation in matrix form as:

$$\boldsymbol{N_S} = \boldsymbol{C}\boldsymbol{\epsilon_R} \tag{14}$$

where $\boldsymbol{C}$ is the composite shell constitutive tensor. A deep assessment of the influence of different beam constitutive modeling methods for thin-walled beams was done by Volovoi et al. (2001).

4. Variational formulation

To derive the equilibrium equations of the problem at hand we make use of the principle of d'Alembert (Meirovitch, 1997). Including the d'Alembert forces and ignoring material damping forces the principle of virtual work for dynamical systems takes the form:

$$\delta \Pi = \delta V - \overline{\delta P}_{\text{ext}} + \overline{\delta K} = 0 \tag{15}$$

where δV is the variation of the strain energy, $\overline{\delta P}_{\text{ext}}$ is the virtual work of the external forces and $\overline{\delta K}$ is the virtual work of the inertia forces.

4.1. Virtual strain energy

Replacing Eq. (12) into Eq. (14) we can express the virtual strain energy as (Washizu, 1968):

$$\delta V = \int_A \delta \boldsymbol{\epsilon}_{\boldsymbol{R}}^{\boldsymbol{T}} \boldsymbol{N}_{\boldsymbol{S}}\, dA = \int_A \delta \boldsymbol{\epsilon}_{\boldsymbol{R}}^{\boldsymbol{T}} \left(\boldsymbol{C}\, \boldsymbol{S}(s)\, \boldsymbol{\epsilon}_{\boldsymbol{G}}(x)\right) dA \tag{16}$$

Therefore:

$$\delta V = \int_A (\boldsymbol{S}\, \delta \boldsymbol{\epsilon}_{\boldsymbol{G}})^{\boldsymbol{T}} \boldsymbol{C}\, \boldsymbol{S} \boldsymbol{\epsilon}_{\boldsymbol{G}}\, dA = \int_A \delta \boldsymbol{\epsilon}_{\boldsymbol{G}}{}^{T} \boldsymbol{S}^{\boldsymbol{T}} \boldsymbol{C}\, \boldsymbol{S} \boldsymbol{\epsilon}_{\boldsymbol{G}}\, dA \tag{17}$$

We define now the following cross-sectional matrix:

$$\boldsymbol{D}_{\boldsymbol{s}} = \boldsymbol{S}^{\boldsymbol{T}} \boldsymbol{C}\, \boldsymbol{S} \tag{18}$$

Replacing Eq. (17) into Eq. (16) and separating the integral we have:

$$\delta V = \int_L \delta \boldsymbol{\epsilon}_{\boldsymbol{G}}{}^{T} \left(\int_S \boldsymbol{D}_{\boldsymbol{s}}\, ds \right) \boldsymbol{\epsilon}_{\boldsymbol{G}}\, dx = \int_L \delta \boldsymbol{\epsilon}_{\boldsymbol{G}}{}^{T} \boldsymbol{D}\, \boldsymbol{\epsilon}_{\boldsymbol{G}}\, dx \tag{19}$$

being:

$$\boldsymbol{D} = \int_{\boldsymbol{s}} \boldsymbol{S}^{\boldsymbol{T}} \boldsymbol{C}\, \boldsymbol{S}\, ds \tag{20}$$

4.2. d'Alembert forces virtual work

The d'Alembert forces virtual work expression is:

$$\delta K = \int_V \rho_0 \delta \boldsymbol{R}^{\boldsymbol{T}} \ddot{\boldsymbol{R}} dV \tag{21}$$

In which $\boldsymbol{R}$ is the position vector of any point in the beam, let's note that $\boldsymbol{R}$ is a function of both the geometry and the instantaneous displacement field. In order to simplify the derivation of $\ddot{\boldsymbol{R}}$ we express the displacement field (Eq. (2) as) as:

$$\boldsymbol{U} = \boldsymbol{S}_{\boldsymbol{M}} \boldsymbol{U}_{\boldsymbol{G}} \tag{22}$$

where the matrix of generalized displacements $\boldsymbol{U}_{\boldsymbol{G}}$ is defined as:

$$\boldsymbol{U}_{\boldsymbol{G}} = \left[u(x,t), v(x,t), w(x,t), \theta_x(x,t), \theta_y(x,t), \theta_z(x,t), \psi(x,t)\right]^{\boldsymbol{T}} \tag{23}$$

and the cross-sectional matrix is:

$$\boldsymbol{S}_{\boldsymbol{M}} = \begin{bmatrix} 1 & 0 & 0 & 0 & -Z(n,s) & -Y(n,s) & F(n,s) \\ 0 & 1 & 0 & -Z(n,s) & 0 & 0 & 0 \\ 0 & 0 & 1 & Y(n,s) & 0 & 0 & 0 \end{bmatrix} \tag{24}$$

The instantaneous position vector of a point in the deformed configuration can be written as:

$$\boldsymbol{R} = \boldsymbol{R}_0 + \boldsymbol{S}_{\boldsymbol{M}} \boldsymbol{U}_{\boldsymbol{G}} \tag{25}$$

where $\boldsymbol{R}_0$ is the point of the beam in the undeformed configuration, this is:

$$\mathbf{R}_0 = [X\ Y\ Z]^T \tag{26}$$

Before proceeding with the formulation of the d'Alembert forces we will introduce the spinor of the angular velocity vector in order to replace the standard cross product for an equivalent matrix product. Being the angular velocity vector:

$$\boldsymbol{\omega} = (\omega_x, \omega_y, \omega_z), \tag{27}$$

its spinor is the following anti-symmetric matrix:

$$\boldsymbol{\Omega} = \begin{bmatrix} 0 & -\omega_z & \omega_y \\ \omega_z & 0 & -\omega_x \\ -\omega_y & \omega_x & 0 \end{bmatrix} \tag{28}$$

Now, for the general case of a structural element that is rotating in space (see Fig. 3) we can write the absolute velocity and acceleration of a point of the beam as:

$$\dot{\boldsymbol{R}} = \boldsymbol{V}(x,n,s,t) = \boldsymbol{V}_{\boldsymbol{01}} + \boldsymbol{V}_{\boldsymbol{R}} + \boldsymbol{\Omega}(\boldsymbol{R}_{\boldsymbol{0}} + \boldsymbol{S}_{\boldsymbol{M}} \boldsymbol{U}_{\boldsymbol{G}}) \tag{29}$$

$$\ddot{\boldsymbol{R}} = \boldsymbol{a}(x,n,s,t) = \boldsymbol{\Omega}(\boldsymbol{\Omega}(\boldsymbol{R}_{\boldsymbol{0}} + \boldsymbol{S}_{\boldsymbol{M}} \boldsymbol{U}_{\boldsymbol{G}})) + \boldsymbol{a}_{\boldsymbol{R}} + 2\boldsymbol{\Omega} \boldsymbol{V}_{\boldsymbol{R}} \tag{30}$$

where $\boldsymbol{V}_{\boldsymbol{R}}$ represents the relative velocity, $\boldsymbol{a}_{\boldsymbol{R}}$ the relative acceleration and $\boldsymbol{\omega}$ the angular velocity vector, readily:

$$\boldsymbol{V}_{\boldsymbol{R}} = \boldsymbol{S}_{\boldsymbol{M}} \boldsymbol{V}_{\boldsymbol{G}} \tag{31}$$

$$\boldsymbol{a}_{\boldsymbol{R}} = \boldsymbol{S}_{\boldsymbol{M}} \boldsymbol{a}_{\boldsymbol{G}} \tag{32}$$

The generalized velocities and accelerations are defined as:

$$\boldsymbol{V}_{\boldsymbol{G}} = \left[\dot{u}(x,t), \dot{v}(x,t), \dot{w}(x,t), \dot{\theta}_x(x,t), \dot{\theta}_y(x,t), \dot{\theta}_z(x,t), \dot{\psi}(x,t)\right]^{\boldsymbol{T}} \tag{33}$$

$$\boldsymbol{a}_{\boldsymbol{G}} = \left[\ddot{u}(x,t), \ddot{v}(x,t), \ddot{w}(x,t), \ddot{\theta}_x(x,t), \ddot{\theta}_y(x,t), \ddot{\theta}_z(x,t), \ddot{\psi}(x,t)\right]^{\boldsymbol{T}} \tag{34}$$

For simplicity, we will consider the velocity of the origin of the rotating coordinate system, namely $\boldsymbol{V}_{\boldsymbol{01}}$, to be zero

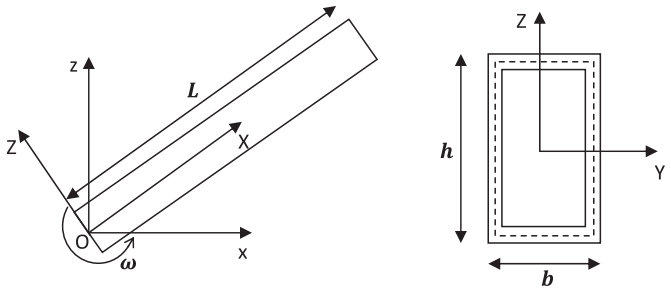

Fig. 3. Rotating beam.

On the other hand, the variation of the position vector is:

$$\delta \boldsymbol{R} = \delta(\boldsymbol{R}_0 + \boldsymbol{S_M U_G}) = \boldsymbol{S_M}\delta\boldsymbol{U_G} \tag{35}$$

Replacing Eqs. (31) and (32) into Eq. (30), using Eq. (35) and recalling the expression of the virtual work of the inertia forces in Eq. (21) we have:

$$\delta K = \int_V \rho_0[\Omega(\Omega(\boldsymbol{R}_0 + \boldsymbol{S_M U_G})) + \boldsymbol{S_M a_G} + 2\Omega(\boldsymbol{S_M V_G})]^{\boldsymbol{T}} \boldsymbol{S_M}\delta\boldsymbol{U_G} dV \tag{36}$$

Reordering and grouping terms we have:

$$\delta K = \rho_0 \Big[\int_V \boldsymbol{\Omega\Omega R}_0 dV + \int_V \boldsymbol{\Omega\Omega S_M U_G} dV + \int_{\mathbf{V}} \mathbf{2}\Omega(\boldsymbol{S_M V_G}) dV + \int_V \boldsymbol{S_M a_G} dV \Big]^{\boldsymbol{T}} \boldsymbol{S_M}\delta\boldsymbol{U_G} \tag{37}$$

4.3. Virtual work of the external forces

The virtual work of external forces can be expressed as:

$$\delta P_{\text{ext}} = \delta \boldsymbol{U}_{\boldsymbol{G}}^T \boldsymbol{F_E} \tag{38}$$

where $\boldsymbol{F_E}$ is a column vector that represents the external forces.

5. Finite element formulation

5.1. Tangent stiffness

Introducing the finite element discretization we can map the generalized strains in generalized nodal displacements. The finite element approximation is (Felippa, 1999; Zienkiewicz and Taylor, 2000):

$$\boldsymbol{U_G} = \boldsymbol{H}\widehat{\boldsymbol{U}} \tag{39}$$

Being; $\boldsymbol{H}$ a matrix of linear shape functions, $\boldsymbol{B}$ the displacement–deformation matrix according to the Green's strain tensor, $\widehat{\boldsymbol{X}}$ the nodal coordinates and $\widehat{\boldsymbol{U}}$ the nodal displacements, we can express the generalized strains matrix $\boldsymbol{\epsilon_G}$ as:

$$\boldsymbol{\epsilon_G} = \boldsymbol{B}\widehat{\boldsymbol{U}} \tag{40}$$

Introducing Eq. (40) in the virtual strain energy expression (Eq. (19)) we obtain:

$$\delta V = \int_{\boldsymbol{L}} \Big(\delta(\boldsymbol{B}\widehat{\boldsymbol{U}})\Big)^{\boldsymbol{T}} \boldsymbol{D}\Big(\boldsymbol{B}\widehat{\boldsymbol{U}}\Big) dx = \int_{\boldsymbol{L}} \delta\widehat{\boldsymbol{U}}^{\boldsymbol{T}} \Big(\boldsymbol{B^T D B}\Big)\widehat{\boldsymbol{U}} dx + \int_{\boldsymbol{L}} \widehat{\boldsymbol{U}}^{\boldsymbol{T}} \delta\boldsymbol{B^T N_B} dx \tag{41}$$

where we have implicitly defined the beam forces vector as:

$$\boldsymbol{N_B} = \boldsymbol{DB}\widehat{\boldsymbol{U}} = \boldsymbol{D}\boldsymbol{\epsilon_G} \tag{42}$$

$$\boldsymbol{N_B} = [N_x, Q_y, Q_z, M_y, M_z, T_{sv}, T_w, B, W]^T \tag{43}$$

To get a closed form expression for the last term of Eq. (39) it is convenient to pass to indicial notation, reverting to matrix notation later upon "index contraction". This is:

$$\int_{\boldsymbol{L}} \widehat{\boldsymbol{U}}^{\boldsymbol{T}} \delta\boldsymbol{B^T N_B} dx = u_j \int_L \frac{\partial B_{ki}}{\partial u_j} \delta u_j N_{Bk} dx \tag{44}$$

whence:

$$K_{Gij} = \int_L \frac{\partial B_{ki}}{\partial u_j} N_{Bk} dx \tag{45}$$

Equation (39) can now be rewritten as:

$$\delta V = \delta\widehat{\boldsymbol{U}}^{\boldsymbol{T}} \boldsymbol{K_M}\widehat{\boldsymbol{U}} + \delta\widehat{\boldsymbol{U}}^{\boldsymbol{T}} \boldsymbol{K_G}\widehat{\boldsymbol{U}} = \delta\widehat{\boldsymbol{U}}^{\boldsymbol{T}} (\boldsymbol{K_M} + \boldsymbol{K_G})\widehat{\boldsymbol{U}} \tag{46}$$

$\boldsymbol{K_M}$ and $\boldsymbol{K_G}$ being the material and geometric stiffness matrices, which are nonlinear functions of the nodal displacements. The term between parentheses is the already known tangent stiffness matrix, readily:

$$\boldsymbol{K_T} = \boldsymbol{K_M} + \boldsymbol{K_G} \tag{47}$$

5.2. Dynamic matrices

Introducing the finite element approximation in Eqs. (26), (33) and (34):

$$\boldsymbol{R_0} = \boldsymbol{H}\widehat{\boldsymbol{X}}, \quad \boldsymbol{V_G} = \boldsymbol{N}\widehat{\boldsymbol{V}}, \quad \boldsymbol{a_G} = \boldsymbol{N}\widehat{\boldsymbol{a}} \tag{48}$$

$\widehat{\boldsymbol{U}}, \widehat{\boldsymbol{V}}$ and $\widehat{\boldsymbol{a}}$ being the nodal displacements, velocities and accelerations respectively. $\boldsymbol{N}$ is the inertia shape functions matrix. We can write the expression (37) as:

$$\delta K = \rho_0 \Big[\int \Omega\Big(\Omega\Big(\boldsymbol{H}\widehat{\boldsymbol{X}}\Big)\Big) dV + \int_V \Omega(\Omega(\boldsymbol{S_M U_G})) dV + \int_{\boldsymbol{V}} 2\Omega\Big(\boldsymbol{S_M N}\widehat{\boldsymbol{V}}\Big) dV + \int_V \boldsymbol{S_M N}\widehat{\boldsymbol{a}} dV \Big] \boldsymbol{S_M N}\delta\widehat{\boldsymbol{U}} \tag{49}$$

Using Eq. (23) we have:

$$\delta K = \rho_0 \Big[\int_V \boldsymbol{\Omega\Omega H}\widehat{\boldsymbol{X}} dV + \int_V \boldsymbol{\Omega\Omega S_M N}\widehat{\boldsymbol{U}} dV + \int_V 2\boldsymbol{\Omega S_M N}\widehat{\boldsymbol{V}} dV + \int_V S_M N\widehat{\boldsymbol{a}} dV \Big]^{\boldsymbol{T}} \boldsymbol{S_M N}\delta\widehat{\boldsymbol{U}} \tag{50}$$

Reordering terms we can express Eq. (50) as:

$$\delta K = \rho_0 \Big[\int_V \widehat{\boldsymbol{X}}^{\boldsymbol{T}} \boldsymbol{H^T \Omega\Omega} dV + \int_V \widehat{\boldsymbol{U}}^{\boldsymbol{T}} \boldsymbol{N^T S_M^T \Omega\Omega} dV + \int_{\boldsymbol{V}} \widehat{\boldsymbol{V}}^{\boldsymbol{T}} \boldsymbol{N^T S_M^T} 2\Omega dV + \int_V \widehat{\boldsymbol{a}}^{\boldsymbol{T}} \boldsymbol{N^T S_M^T} dV \Big] \boldsymbol{S_M N}\delta\widehat{\boldsymbol{U}} \tag{51}$$

Finally:

$$\delta K = \rho_0 \Big[\int_V \widehat{\boldsymbol{X}}^{\boldsymbol{T}} \boldsymbol{H^T \Omega\Omega S_M N} dV + \int_V \widehat{\boldsymbol{U}}^{\boldsymbol{T}} \boldsymbol{N^T S_M^T \Omega\Omega S_M N} dV + \int_{\boldsymbol{V}} \widehat{\boldsymbol{V}}^{\boldsymbol{T}} \boldsymbol{N^T S_M^T} 2\boldsymbol{\Omega S_M N} dV + \int_V \widehat{\boldsymbol{a}}^{\boldsymbol{T}} \boldsymbol{N^T S_M^T S_M N} dV \Big] \delta\widehat{\boldsymbol{U}} \tag{52}$$

Since the nodal values are not a function of the longitudinal coordinate, the last expression can be rewritten for an element as:

$$\delta K_e = \left(\boldsymbol{F_C}\widehat{\boldsymbol{X}} + \boldsymbol{K_R}\widehat{\boldsymbol{U}} + \boldsymbol{C_C}\widehat{\boldsymbol{V}} + \boldsymbol{M}\widehat{\boldsymbol{a}}\right)\delta\widehat{\boldsymbol{U}} \tag{53}$$

It must be noted that $\boldsymbol{F_C}$ is the centrifugal load vector, $\boldsymbol{K_R}$ is the rotation stiffness matrix, $\boldsymbol{C_C}$ is the Coriolis matrix and $\boldsymbol{M}$ is the consistent mass matrix:

$$\begin{aligned}
\boldsymbol{F_C} &= \rho_0 \int_{V_e} \boldsymbol{H^T \Omega \Omega S_M N} dV_e \\
\boldsymbol{K_R} &= \rho_0 \int_{V_e} \boldsymbol{N^T S_M^T \Omega \Omega S_M N} dV_e \\
\boldsymbol{C_C} &= \rho_0 \int_{\boldsymbol{V}} \boldsymbol{N^T S_M^T} 2\boldsymbol{\Omega S_M N} dV \\
\boldsymbol{M} &= \rho_0 \int_{V} \boldsymbol{N^T S_M^T S_M N} dV
\end{aligned} \tag{54}$$

The centrifugal load vector can be treated as an external load.

6. Dynamic stability

6.1. Equations of motion

Introducing the finite element version of Eq. (37) and Eqs. (44) and (53) in Eq. (15), assuming conservative loading and using the arbitrariness condition of the virtual magnitudes, as well as the satisfaction of the boundary conditions, we can formulate the equations of motion in matrix form as:

$$(\boldsymbol{K_M} + \boldsymbol{K_G} + \boldsymbol{K_R})\widehat{\boldsymbol{U}} + \boldsymbol{C_C}\widehat{\boldsymbol{V}} + \boldsymbol{M}\widehat{\boldsymbol{a}} = -\boldsymbol{F_C} + \boldsymbol{F_E} \tag{55}$$

Ignoring Coriolis forces the equations of motion reduce to:

$$(\boldsymbol{K_M} + \boldsymbol{K_G} + \boldsymbol{K_R})\widehat{\boldsymbol{U}} + \boldsymbol{M}\widehat{\boldsymbol{a}} = -\boldsymbol{F_C} + \boldsymbol{F_E} \tag{56}$$

Although the vector of centrifugal loads $\boldsymbol{F_C}$ is obtained from the d'Alembert forces it can be thought as an external static force (function of the longitudinal coordinate), for that reason it has been written in the right hand side of the equation above. Although defined positive for simplicity, it's very important to note that the rotation stiffness matrix actually plays the role of a negative stiffness. The negative sign in the diagonal terms of $\boldsymbol{K_R}$ appears from the spinor product $\boldsymbol{\Omega\Omega}$, the same occurs with the centrifugal load vector.

In this paper the dynamic stability of a beam subjected to axial loads is studied. Since for the analyzed beam the axial natural frequencies are very high compared with those exited parametrically we will neglect the axial inertia forces when calculating the axial beam force. Thus, the resultant axial beam force equals to the axial external load.

We will consider the problem to be an initial stress problem. Following the steps of Section 5.1 for the derivation of the geometric stiffness matrix we found that it is possible to express the geometric stiffness matrix as:

$$\boldsymbol{K_G} = T\,\boldsymbol{K_G^U} \tag{57}$$

where T is the axial beam force at the element centroids and $\boldsymbol{K_G^U}$ is a unit geometrical stiffness matrix. For a seven DOF per node element with linear shape functions $\boldsymbol{K_G^U}$ yields:

$$\boldsymbol{K_G^U} = \begin{bmatrix}
0 & 0 & 0 & 0 & 0 & 0 & 0 & 0 & 0 & 0 & 0 & 0 & 0 \\
0 & 1 & 0 & 0 & 0 & 0 & 0 & 0 & -1 & 0 & 0 & 0 & 0 \\
0 & 0 & 1 & 0 & 0 & 0 & 0 & 0 & 0 & -1 & 0 & 0 & 0 \\
0 & 0 & 0 & I_o & 0 & 0 & 0 & 0 & 0 & 0 & -I_o & 0 & 0 \\
0 & 0 & 0 & 0 & 0 & 0 & 0 & 0 & 0 & 0 & 0 & 0 & 0 \\
0 & 0 & 0 & 0 & 0 & 0 & 0 & 0 & 0 & 0 & 0 & 0 & 0 \\
0 & 0 & 0 & 0 & 0 & 0 & 0 & 0 & 0 & 0 & 0 & 0 & 0 \\
0 & 0 & 0 & 0 & 0 & 0 & 0 & 0 & 0 & 0 & 0 & 0 & 0 \\
0 & -1 & 0 & 0 & 0 & 0 & 0 & 1 & 0 & 0 & 0 & 0 & 0 \\
0 & 0 & -1 & 0 & 0 & 0 & 0 & 0 & 1 & 0 & 0 & 0 & 0 \\
0 & 0 & 0 & -I_o & 0 & 0 & 0 & 0 & 0 & I_o & 0 & 0 & 0 \\
0 & 0 & 0 & 0 & 0 & 0 & 0 & 0 & 0 & 0 & 0 & 0 & 0 \\
0 & 0 & 0 & 0 & 0 & 0 & 0 & 0 & 0 & 0 & 0 & 0 & 0 \\
0 & 0 & 0 & 0 & 0 & 0 & 0 & 0 & 0 & 0 & 0 & 0 & 0
\end{bmatrix} \tag{58}$$

Where I_o is the polar moment of inertia divided by the area, that is:

$$I_o = \frac{\int_A \left(Y^2 + Z^2\right) dA}{A} \tag{59}$$

6.2. Dynamic stability

We derive in this section the equation of motion of a rotating cantilever beam subjected to an axial excitation of the form:

$$P(t) = P_s + P_d \cos(\theta t) \tag{60}$$

where θ is the excitation frequency, $P_s = \alpha P_{\mathrm{cr}}$ and $P_d = \beta P_{\mathrm{cr}}$, α is the static load factor, β is the dynamic load factor and P_{cr} is the critical load of the beam.

Since both external forces acting on the beam are longitudinal and having in mind Eq. (60) and Eq. (57), we write the equations of motion (Eq. 56) as:

$$(\boldsymbol{K_M} + \boldsymbol{K_R} + (N_R - P(t))\boldsymbol{K_G^U})\widehat{\boldsymbol{U}} + \boldsymbol{M}\widehat{\boldsymbol{a}} = 0 \tag{61}$$

$\widehat{i}$ being the versor representing the axial degree of freedom. N_R represents the axial force in the element caused by the rotation. For a finite element of constant cross-sectional area, and x_c being the element centroid coordinate (measured from the origin of the axis of rotation), we have:

$$N_R = \rho A_e |\boldsymbol{\omega}|^2 \frac{1}{2}\left(L_e^2 - x_c^2\right) \tag{62}$$

Here the axis of rotation intersects the beam's reference line.

When the beam is excited in the axial (longitudinal) direction, and the interaction of this movement with the other motions is studied, the coupling of these various motions depends on the symmetry of the cross-section.

6.3. Principal parametric resonance

In the classification of parametric resonance, if θ is the excitation frequency and ω_1 the natural frequency of the ith mode, parametric resonance of "first kind" is said to occur when $\theta/2\omega_1 \cong 1/r,\ r = 1, 2\ldots$, while parametric resonance of the "second kind" is said to occur when $\theta/(\omega_j \pm \omega_j) \cong 1/r,\ r = 1, 2\ldots\ (k \neq j)$. In both cases the situation where $r = 1$ is generally the only one of practical importance. Usually the parametric resonance of the first kind is termed "parametric resonance", whereas the second kind is referred as "combination resonance", because it involves two different

Table 1
Natural frequencies (Hz). Abaqus vs. present theory.

Model validation						
Laminate	Abaqus			Present theory		
	ω_S	ω_D	ω_D^α	ω_S	ω_D	ω_D^α
{0,0,0,0}	7.17	14.16	10.40	7.32	14.48	10.54
	13.50	18.60	15.89	13.56	18.77	15.92
	31.79	37.21	36.62	32.16	35.59	34.71
	34.32	53.49	46.24	37.04	55.58	48.27
	62.60	71.85	67.52	63.53	74.02	69.29
{0,90,90,0}	5.42	11.08	8.27	5.47	11.59	8.40
	10.22	17.69	16.35	10.24	18.13	16.37
	28.56	36.87	36.76	30.08	35.48	34.91
	31.87	48.83	44.85	32.03	51.18	45.81
	52.55	62.29	61.19	53.12	65.18	61.53
{45,−45,−45,45}	2.54	6.92	5.15	2.48	7.26	5.23
	4.77	17.34	16.78	4.69	17.41	16.72
	15.94	44.36	41.78	15.44	44.54	41.58
	29.54	46.73	44.61	29.03	48.06	45.59
	44.79	79.32	76.16	42.91	80.57	76.84

frequencies. In this paper the study is only concentrated in the case of parametric resonance.

The process of finding the boundaries of the regions of instability consist on the determination of the conditions under which the differential equation of the system, namely Eq. (35), has periodic solutions with period $2\pi/\theta$ and $4\pi/\theta$. For the principal region, which is a half subharmonic, one looks for a solution with a period which is twice the forcing frequency: i.e., $4\pi/\varpi$. The condition for the existence of solutions can be expressed in the following infinite determinant form (Bolotin, 1964):

$$\begin{bmatrix} \boldsymbol{K}+(\overline{P}\pm P_d)\boldsymbol{K_G^U}-\frac{1}{4}\theta^2\boldsymbol{M} & -\frac{1}{2}P_d\boldsymbol{K_G^U} & 0 & \cdots \\ & \boldsymbol{K}+\overline{P}\boldsymbol{K_G^U}-\frac{9}{4}\theta^2\boldsymbol{M} & -\frac{1}{24}P_d\boldsymbol{K_G^U} & \cdots \\ SYM & & \boldsymbol{K}+\overline{P}\boldsymbol{K_G^U}-\frac{25}{4}\theta^2\boldsymbol{M} & \cdots \\ \cdots & \cdots & \cdots & \cdots \end{bmatrix} = 0$$

Where: (63)

$$\overline{P} = (N_R - P_s) \tag{64}$$

$$\boldsymbol{K} = \boldsymbol{K_M} + \boldsymbol{K_R} \tag{65}$$

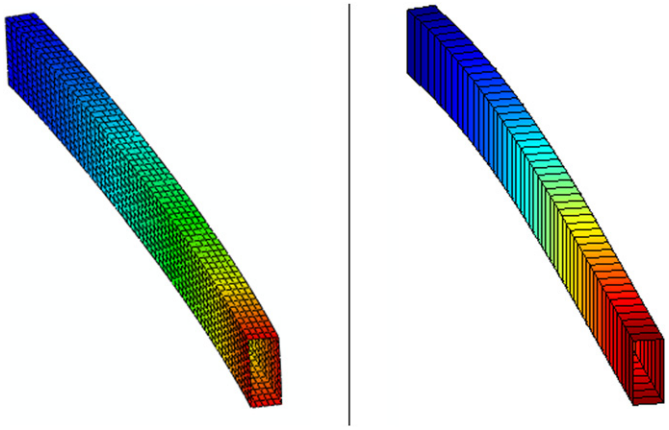

Fig. 4. First mode shape – Shell model (Abaqus) vs. present beam model (Matlab).

Table 2
Natural frequencies and critical loads.

Bisymmetric box beam – Elements = 50.						
Laminate	P_{CR}^S (N)	P_{CR}^D (N)	ω_S	ω_D	ω_D^α	Mode
{0,0,0,0}	2.1359×10^7	2.1711×10^7	25.93	26.16	19.42	Flap 1
			45.67	45.68	42.64	Lag 1
			65.20	65.27	63.76	Tors 1
			101.00	101.36	91.53	Flap 2
			163.71	163.91	158.23	Lag 2
{0,90,90,0}	1.2441×10^7	1.2792×10^7	20.39	20.69	15.20	Flap 1
			36.88	36.89	34.41	Lag 1
			64.74	64.81	63.92	Tors 1
			89.76	90.15	83.43	Flap2
			147.96	148.16	144.38	Lag 2
{45,−45,−45,45}	2.6825×10^6	3.0330×10^6	9.87	10.52	7.60	Flap 1
			18.64	18.69	17.27	Lag 1
			60.54	61.11	58.20	Flap 2
			110.91	111.16	109.268	Lag 2
			164.13	164.38	164.29	Axial 1

The boundaries of the instability regions lying near $\theta = 2\omega_1$ can be determined with sufficient accuracy considering the first leading diagonal term (Bolotin, 1964):

$$|\boldsymbol{K_M} + \boldsymbol{K_R} + (N_R - P_s \pm P_d)\,\boldsymbol{K_G^U} - \frac{1}{4}\theta^2\boldsymbol{M}| = 0 \tag{66}$$

To scale the results of Eq. (64) with the corresponding frequencies and critical loads it's necessary to solve additionally three eigen problems; the problem of free vibration of an unloaded rotating beam:

$$|\boldsymbol{K_M} + \boldsymbol{K_R} - \omega^2\boldsymbol{M}| = 0, \tag{67}$$

the problem of free vibration of a beam loaded by a constant longitudinal force

$$|\boldsymbol{K_M} + \boldsymbol{K_R} + (N_R - P_s \pm P_d)\boldsymbol{K_G^U} - \omega^2\boldsymbol{M}| = 0, \tag{68}$$

And finally, the buckling problem:

$$|\boldsymbol{K_M} + \boldsymbol{K_R} + (N_R - P_s \pm P_d)\boldsymbol{K_G^U}| = 0 \tag{69}$$

7. Applications and numerical results

We are mainly interested in the effects of the angular velocity and the laminate stacking sequence on the natural frequencies of the beam and its instability regions. We will base the numerical implementation on a bisymmetric closed cross-section, considering different laminate schemes. The analyzed material is graphite-epoxy (AS4/3501) whose properties are $E_1 = 144$ GPa, $E_2 = 9.65$ GPa, $G_{12} = 4.14$ GPa, $G_{13} = 4.14$ GPa, $G_{23} = 3.45$ GPa, $\nu_{12} = 0.3$, $\nu_{13} = 0.3$, $\nu_{23} = 0.5$, $\rho = 1389$ kg/m^3.

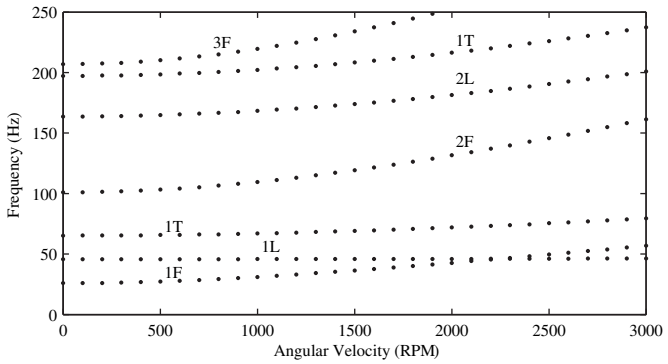

Fig. 5. Modal interchange for a {0/0/0/0} laminate.

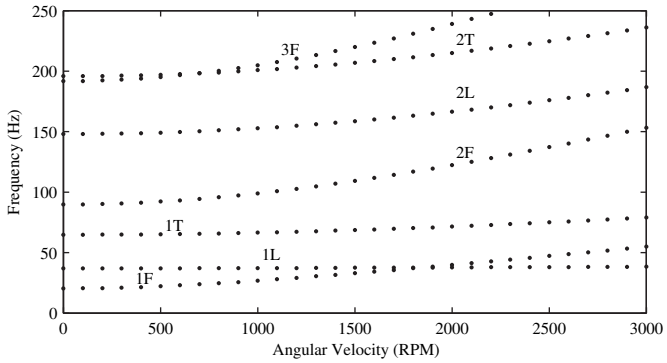

Fig. 6. Modal interchange for a {0/90/90/0} laminate.

In all the results presented below, the value of the static load parameter is adopted $\alpha = 0.5$, and the excitation frequency θ is scaled with the lowest frequency value of parametric resonance (that is the double of the fundamental natural frequency, that is: $2\omega_1$). It's worth to note that for all cases studied in this paper the angular velocity has only one component, that is $\boldsymbol{\omega} = \omega_y \hat{j}$.

7.1. Beam model validation

In order to validate the beam finite element we compare natural frequencies of a rotating preloaded beam using the present theory vs. a 3D shell model in Abaqus. To compare both formulations we use a graphite-epoxy (AS4/3501) box beam, its geometric properties are: length $L = 10$ m, height $h = 0.7$ m, width $b = 0.3$ m and thickness $e = 0.05$ m. The beam is rotating at 1000 rpm and is preloaded with half the first critical buckling load.

The Abaqus model was studied through a multistep analysis using the geometrical nonlinear flag to carry the strain and stress states through subsequent steps. The beam was discretized using 1800 four-noded shell elements (S4) and the rotation effects were added to the model through the *CENTRIF load label. The natural frequencies were extracted with the *SUBSPACE eigensolver.

Table 1 shows the comparison in natural frequencies in Hz for different load cases, ω_S andω_D represent the natural frequencies of the beam without rotation and a beam rotating at 1000 rpm, respectively. Finally, ω_D^{α} represents the natural frequency considering both the rotation effects and the static load. The implementation of the beam model was done in Matlab and, for a better visualization; the whole cross-section movement was rendered.

It is observed that the natural frequencies obtained with the present beam model have a good correlation with that obtained with 3D shell model. As expected, the frequencies increase with the angular velocity and decrease with the compressive load. It's important to note that to avoid possible confusions generated by the inversion in the mode ordering, a description of the corresponding modes was not added to Table 1. This phenomenon will be described in detail in the next sections. The maximum differences between the two models are observed for superior modes, these differences are never higher that 5%. Considering the latter, we can state that the present model is validated. The analysis of the variation of the natural frequencies with the rotational speed and the preload is essential to characterize the dynamic instability behavior of the beam.

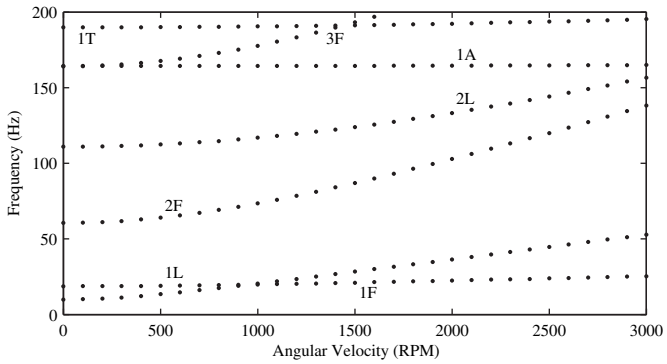

Fig. 7. Modal crossing for a {45/−45/−45/45} laminate.

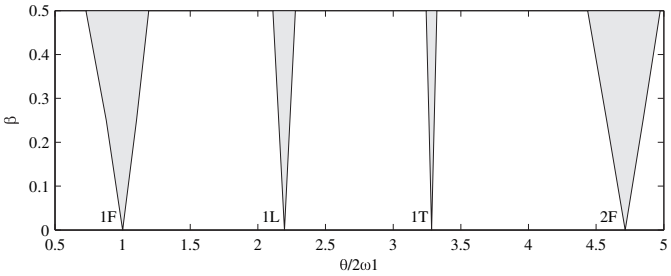

Fig. 8. Instability regions for a {0/0/0/0} laminate.

Fig. 4 shows a comparison of the first mode of vibration between the 3D shell and the present beam model.

7.2. Natural frequencies and modal interchange

We study in this section a cantilever beam with a bisymmetric box cross-section whose geometric properties are: $L = 5$ m, $h = 0.7$ m, $b = 0.3$ m, $e = 0.05$ m. Note that because of the cross-section symmetry the motion equations are uncoupled. Therefore, there are three main modes of vibration: flapping, lagging and torsional. Table 2 shows the natural frequencies and critical loads of the beam for different load cases, P_{CR}^{S} represents the critical load of the beam without considering the rotation effects and P_{CR}^{D} is the critical load of the beam considering the rotation effects, both units being Newtons. As in the previous case, ω_S andω_D represent the natural frequencies of the beam without rotation and a beam rotating at 200 rpm, respectively. Finally, ω_D^{α} represents the natural frequency considering the rotation effects (200 rpm) and the static load.

The critical load observed in Table 2 corresponds to a flexural mode in the y direction. It can be seen that the effect of rotation increases the buckling load, specially for the most flexible laminate ({45,−45,−45,45}). A similar behavior is observed for the natural frequencies of an unloaded beam. The longitudinal lamination sequence, namely {0,0,0,0}, gives the highest frequencies for both the static and the rotating beam. Conversely, the laminate {45,−45,−45,45} presents the lowest frequency values. As expected, the effect of the static load ($\alpha = 0.5$) reduces the natural frequency of a rotating beam. However, this effect depends on the beam

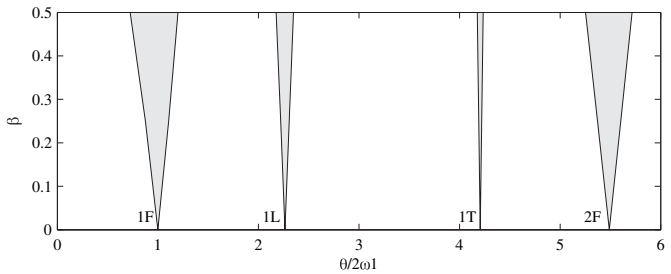

Fig. 9. Instability regions for a {0/90/90/0} laminate.

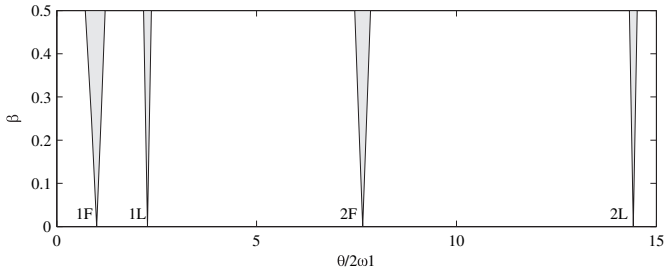

Fig. 10. Instability regions for a {45/−45/−45/45} laminate.

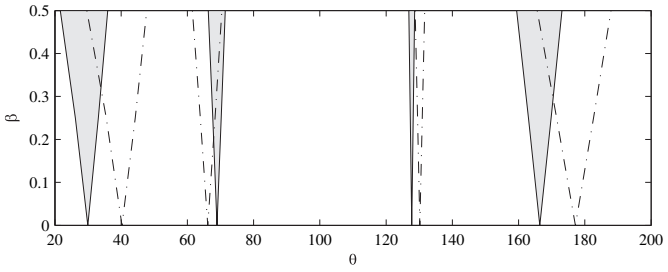

Fig. 12. Instability regions for a {0/90/90/0} laminate.

vibration mode, i.e., the natural frequency reduction is larger in the first mode (Flapping 1, 26% reduction). This effect keeps almost constant for the different laminates.

In order to analyze the modal behavior of the rotating beam we plot the first seven natural frequencies of an unloaded beam vs. the angular velocity. Figs. 5–7 show the results for the *{0,0,0,0}*, *{45,−45,−45,45}* and *{0,90,90,0}* laminates respectively.

As it can be observed, the curves show that the natural frequencies increase with the angular frequency. This increase depends not only on the mode but also on the laminate stacking sequence. It was found that there are critical angular velocities for which a modal interchange phenomenon can exist. As it can be seen from Fig. 5, in the laminate *{0/0/0/0}* the first flapping and first lagging modes cross each other at about 2300 rpm. This modal interchange of the first modes is generated because the first lagging mode is practically not affected by the rotational speed. This lack of sensitivity of the first lagging mode to the angular velocity variation is observed for all the laminates studied in this paper.

In the case of the laminate {*0/90/90/0*}, the dynamic behavior of the first modes is similar to the previous laminate. The frequency curves show that the rotation stiffening effect is more significant in the flapping modes. This causes two modal interchanges; the first flapping with the first lagging modes at 1800 rpm and the third flapping and second torsional modes at about 700 rpm.

The modal interchange phenomenon is more evident for the laminate *{45/−45/−45/45}*. In this case the torsional mode has a high frequency and the first axial mode appears before. Also, both modes are not strongly affected by the rotation, and thus, two additional modal interchanges appear. At about 1000 rpm the first flapping mode crosses over the first lagging mode. Also, since the third flapping mode is strongly affected by the rotation, it crosses the first axial mode at 50 rpm and the first torsional mode at about 1450 rpm. By coincidence, the first axial and the third flapping modes have almost the same frequency for the beam without rotation.

7.3. Instability regions

In this section we study the behavior of the instability regions for different laminate sequences. Figs. 8–10 show the instability regions for three laminates: {*0/0/0/0*}, *{45/−45/−45/45}* and *{0/90/90/0}*, and for a rotational speed of 200 rpm. It is observed that the widest regions of instability correspond to parametrically excited flapping modes. Remember that θ is the excitation frequency, α is the static load factor and β is the dynamic load factor, see Eq. (60).

The region corresponding to parametrically excited torsional modes is more distant from the main region in the case of the laminate *{0,90,90,0}*, in comparison with the laminate *{0,0,0,0}* (see Fig. 9). For the laminate *{45,−45,−45,45}* the torsional mode is stiffer than the second lagging mode, for that reason it wasn't showed in Fig. 10.

To show the effect of the rotational speed on the instability boundaries we compare the instability regions of a beam without rotation with a beam rotating at 1000 rpm (see Figs. 11–13). The stability region corresponding to the rotating beam is plotted in dotted-dashed line while the no rotation case is plotted in solid line. For clearness, we have not scaled the forcing frequency. Fig. 11 shows the evolution of the instability regions for the case of a laminate {*0/0/0/0*}. It's observed that the effect of rotation not only moves the regions but also makes it wider.

We previously stated that an increase in the angular velocity of the beam leads to an increase in the natural frequencies of the beam. In contrast to what could be expected, not all regions move to the right when increasing the rotational speed. For the particular case of the {*0/0/0/0*} and {*0/90/90/0*} laminates, the region corresponding to the first lagging mode moves to the left. This occurs because the angular velocity influences the critical buckling load but not the first lagging mode natural frequency.

The laminate *{0/90/90/0}* shows a very similar instability behavior to that of the previous laminate, see Fig. 12. It is important to note that for these two laminates the ordering of parametrically excited regions is the same to that obtained in the case of an angular velocity of 200 rpm (Table 2).

In the case of a laminate *{45/−45/−45/45}* (Fig. 13), the angular velocity effect strongly increases the unstable regions size. Moreover, for the first two regions the influence of this effect provokes the regions to cross each other. This effect is observed because for the angular speed for which the dash-dotted regions where plotted (1000 rpm) a modal interchange between the first flapping and first lagging mode has just occurred.

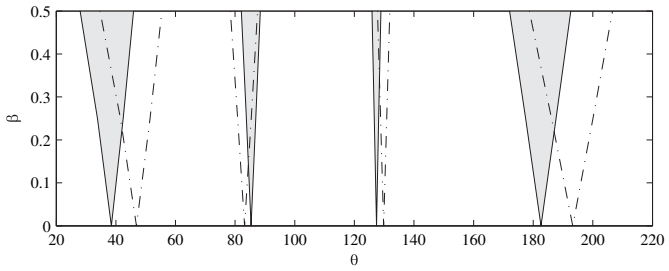

Fig. 11. Instability regions for a {0/0/0/0} laminate.

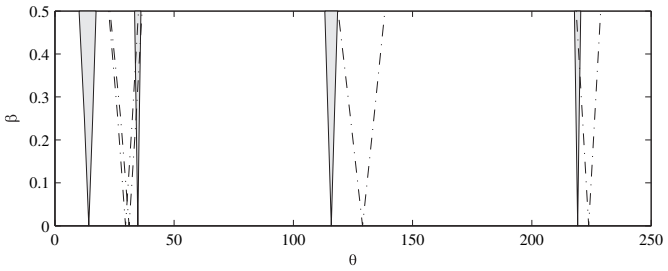

Fig. 13. Instability regions for a {45/−45/−45/45} laminate.

8. Conclusions

In this paper the dynamic stability of a rotating beam was studied and a finite element was specially formulated for that purpose. As a distinct aspect, the beam formulation incorporates in a full form the effect of shear deformation, warping inhibition and rotary inertia. The instability behavior of a cantilever beam subjected to axial load was obtained by means of the Bolotin's method. The dynamic stability problem was formulated by means of linearization of a geometrically nonlinear Total Lagrangian finite element that takes into account the rotation effects.

The numerical results show that the natural frequencies depend highly on the rotational speed. Also, the influence of this effect depends on the laminate stacking sequence analyzed. For example, the stiffening effect of the angular velocity is larger for the laminate *{45,−45,−45,45}*. On the other hand, for some laminations and at different angular velocities of the beam a modal interchange phenomenon can appear. This phenomenon is more frequently observed for the first flapping and lagging modes, mainly because the first lagging mode is almost independent of the rotation speed.

The unstable regions shift to the right when increasing the angular velocity and the size of these regions is also influenced by the angular velocity. Also, the unstable boundaries are affected by the variation of the orientation angle of the laminate fibers.

For the box cross-section analyzed the widest regions of instability correspond to parametrically excited flapping modes. In contrast, the smallest regions correspond to parametrically excited torsional modes.

Acknowledgements

The authors wish to acknowledge the supports from Secretaría de Ciencia y Tecnología of Universidad Tecnológica Nacional and CONICET.

References

Abbas, B.A.H., 1986. The dynamic stability of a rotating Timoshenko beam with a flexible root. Journal of Sound and Vibration 60, 33–44.
Barbero, E.J., 1999. Introduction to Composite Material Design. Taylor and Francis, London.
Bolotin, V.V., 1953. On the parametric excitation of transverse vibrations. Transverse Vibrations and Critical Velocities 2, 5–44. Collection of papers.
Bolotin, V.V., 1964. The Dynamic Stability of Elastic Systems. Holden-Day, San Francisco.
Chen, L.W., Peng, W.-K., 1995. Dynamic stability of rotating blades with geometric non-linearity. Journal of Sound and Vibration 187 (3), 421–433.
Chen, L.W., Peng, W.K., 1998. Dynamic stability of rotating composite shafts under periodic axial compressive loads. Journal of Sound and Vibration 212, 215–230.
Cortínez, V.H., Piovan, M.T., 2002. Vibration and buckling of composite thin-walled beams with shear deformability. Journal of Sound and Vibration 258 (4), 701–723.
Evan-Iwanowski, R.M., 1965. On the parametric response of structures. Applied Mechanics Review 18, 699–702.
Felippa, C., 1999. Lecture Notes in Nonlinear Finite Element Methods. Report No. CU-CSSC-99-xx. Center of Aerospace Structures, University of Colorado.
Ghobarah, A.A., Tso, W.K., 1972. Parametric stability of thin-walled beams of open section. Journal of Applied Mechanics 39, 201–206.
Goldenblat, I.I., 1947. Contemporary Problems of Vibrations and Stability of Engineering Structures. Stroiizdat, Moscow.
Gürgöze, M., 1985. On the dynamic stability of pre-twisted beam subject to a pulsating axial load. Journal of Sound and Vibration 102, 415–422.
Hasan, S.A., Barr, A.D.S., 1974. Non-linear and parametric vibration of thin-walled beams of equal angle-section. Journal of Sound and Vibration 31, 25–47.
Librescu, L., 2006. Thin-Walled Composite Beams. Springer, Dordrecht.
Machado, S.P., Cortínez, V.H., 2005. Non-linear model for stability of thin-walled composite beams with shear deformation. Thin-Walled Structures 43, 1615–1645.
Machado, S.P., Cortínez, V.H., 2007. Parametric vibration of thin-walled composite beams with shear deformation. Journal of Sound and Vibration 305, 563–581.
Meirovitch, L., 1997. Principles and Techniques of Vibrations. Prentice Hall, New Jersey.
Mettler, E., 1962. Dynamic Buckling, Handbook of Engineering Mechanics. McGraw-Hill, New York.
Nayfeh, A.H., Mook, D.T., 1979. Nonlinear Oscillations. Wiley, New York.
Piovan, M.T., Cortínez, V.H., 2005. Transverse shear deformability in the dynamics of thin-walled composite beams, consistency of different approaches. Journal of Sound and Vibration 285, 721–733.
Popelar, C.H., 1972. Dynamic stability of thin-walled column. Journal of the Engineering, Mechanics Division, Proceedings of the American Society of Civil Engineers 98, 657–677.
Sakar, G., Sabuncu, M., 2003. Dynamic stability of a rotating asymmetric cross-section subjected to an axial periodic force. International Journal of Mechanical Sciences 45, 1467–1482.
Tso, W.K., 1968. Parametric torsional stability of a bar under axial excitation. Journal of Applied Mechanics 35, 13–19.
Volovoi, V.V., Hodges, D.H., Cesnik, C.E.S., Popescu, B., 2001. Assessment of beam modeling methods for rotor blade applications. Mathematical and Computer Modelling vol. 33 (No. 10–11), 1099–1112.
Washizu, K., 1968. Variational Methods in Elasticity and Plasticity. Pergamon Press, Oxford.
Zienkiewicz, O.C., Taylor, R.L., 2000. The Finite Element Method, vol. II. Butterworth-Heinemann.